Front. Earth Sci. 2021, 15(4): 876–891
https://doi.org/10.1007/s11707-021-0908-7

RESEARCH ARTICLE

Discriminating hydrocarbon generation potential of coaly source rocks and their contribution: a case study from the Upper Paleozoic of Bohai Bay Basin, China

Jinjun XU[1], Da LOU (✉)[1,2], Qiang JIN[1], Lixin FU[2], Fuqi CHENG[1], Shuhui ZHOU[2], Xiuhong WANG[3], Chao LIANG[1], Fulai LI[1]

1 Shandong Provincial Key Laboratory of Deep Oil and Gas, Qingdao 266580, China
2 PetroChina Dagang Oilfield Company, Tianjin 300280, China
3 Research Institute of Petroleum Exploration and Development, Shengli Oilfield Company, Sinopec, Dongying 257015, China

Abstract Although various coaly source rocks widely developed in the Carboniferous–Permian (C–P) of the Bohai Bay Basin, their geochemical characteristics and hydrocarbon generation potential are poorly understood. This study aims to discriminate the contribution of hydrocarbon generation from different C–P coaly source rocks and clarify the differences within generated oils using organic geochemistry, organic petrology, and thermal simulation experiments. The coaly source rocks containt coal clarain and durain, carbonaceous shale, and shale deposited in deltaic and lagoonal environment. The results indicated that clarain, durain, and carbonaceous shale exhibited higher hydrogen index and liquid–gas hydrocarbon yields than lagoonal and deltaic shales, which was mainly associated with the concentrations of sporinite, cutinite, and hydrogen-rich collodetrinite. Aliphatic hydrocarbons originated from coal and carbonaceous shale presented lower Ts/(Ts + Tm), Ga/17α(H)21β(H)-C_{30} hopane, 18α(H)-oleanane/17α(H)21β(H)-C_{30} hopane ratios, and higher 17β(H)21α(H)-C_{30} Morane/17α(H)21β(H)-C_{30} hopane than deltaic lagoonal shales. Parameters of aromatic hydrocarbons generated from five lithologies of coaly source rocks trended as clear group distribution, e.g., clarain and durain showing lower MNR, DBT/Fluorene (F) ratios and higher DBF/F ratio than coaly shales. The distinct descending trend of hydrocarbon potential is obtained from clarain, durain, carbonaceous shale to lagoonal and deltaic shales, implying dominated the petroleum and natural gas supplement from coal and carbonaceous shale. The difference between aliphatic and aromatic hydrocarbons provides a significant contribution to analyze the generic relationship between coaly source rock and lacustrine shale. Our results illustrate the importance of coaly source rocks for the in-depth oil-gas exploration of the Bohai Bay Basin and understanding hydrocarbon generation potential of source rocks in coal bearing strata.

Keywords thermal simulation, hydrocarbon generation, coaly source rock, Carboniferous–Permian, Bohai Bay Basin

1 Introduction

Carboniferous–Permian (C–P) coal-bearing strata is of high potential for petroleum generation, which has been discovered in several basins worldwide (e.g., Ordos Basin in China, Stellarton Sub-basins in Canada, and coal seam strata in Kansas of America) (Collinson et al., 1994; Ahmed et al., 2009; D'Angelo et al., 2010; Li et al., 2016, 2019a; Wang et al., 2016). Coaly source rocks occurred in the Bohai Bay Basin and Ordos Basin have been found to generate large amounts of hydrocarbons, with several large gas fields has been successfully developed in Ordos Basin (Jin et al., 2009; Tang et al., 2012; Zhao et al., 2018; Li et al., 2020). Even though gas exploration breakthroughs from the Bohai Bay Basin have been achieved, commercial production of oil and gas generated from the coaly strata has not been fully understood.

The evaluation of C–P coaly source rocks has received considerable attention in recent decades (Li et al., 2016, 2019b). C–P coaly source rocks were considered to be deposited in a transitional environment, and consist of coal, mudstone, carbonaceous shale, and dark shale (Collinson et al., 1994; D'Angelo et al., 2010; Figueiredo

Received February 23, 2021; accepted May 12, 2021

E-mail: louda@petrochina.com.cn

et al., 2010; Zhao et al., 2015; Wang et al., 2016). C–P coal seams were believed as good source rocks providing abundant hydrocarbons (Wang et al., 2016; Zhao et al., 2018). The coaly source rocks have been assessed in terms of several aspects, including hydrocarbon generation history, maceral components, thermal simulation experiments, and oil-source relationships (Figueiredo et al., 2010; Tewari and Khan, 2015; Wang et al., 2016; Zhao et al., 2018). The total organic carbon (TOC) content of coal presented a wide variation between 20.5 wt% and 75.0 wt% (Wang et al., 2016; Zhao et al., 2018). The majority of coaly source rocks have higher hydrocarbon potentials implying good quality, whereas that of carbonaceous shales and dark shale ranges from low to good (He et al., 2016; Zhao et al., 2018). Type III to Type II_2 kerogen with the minority featuring Type II_1 are generally found in the the coaly source rocks (Zhao et al., 2018). The differences in the organic matter abundance of coaly source rocks are revealed by observations of maceral components.

Many studies of coal petrology show that the coaly source rocks mainly comprise collodetrinite, collotelinite, corpogelinite, inertinite, and a small amount of liptinite (Michelsen and Khorasani, 1990; Stasiuk, 1994; Tewari and Khan, 2015). Jin et al. (2009) and Zeng et al. (2013) revealed that a considerable amount of natural gas could be extracted from the C–P coaly source rocks, such as from well GBG1 of Jiyang Depression and well WL3 of Dongpu Sag in the Bohai Bay Basin. Furthermore, the occurrence of large amounts of hydrogen-rich collodetrinites and liptinite (e.g., cutinite, sporinite, and resinite) is expected to enhance coaly source rocks generating more hydrocarbons, especially in clarain, durain, and certain mudstones (Tewari and Khan, 2015). More vitrinite and liptinite were found in coal deposited in the Argonne premium coal set and Cantabrian–Barruelian coal seams (Hartgers et al., 1994; Colmenero et al., 2008). Moreover, a high predominance of isomers with linear carbon skeletons speculated to be derived from microorganisms to vitrinite precursor sources was observed (Hartgers et al., 1994).

In agreement with these findings, along with the large-scale generation of coal-derived gas, large estimates of condensate and crude oils have been determined in the Bohai Bay Basin (Kędzior, 2009; Zhao et al., 2018). For example, coal-derived petroleum reservoirs have been detected in well KG4 and well SU23 in the Bohai Bay Basin (Ryder et al., 2012; Zhao et al., 2018). In particular, with the recent major discovery of coaly-related condensate from wells YG1 and QG8 in the Bohai Bay Basin, coaly source rocks presenting better hydrocarbon potential are attracting wide attention (Zhao et al., 2018). Jin et al. (2009) and Zhao et al. (2018) pointed out that coaly source rocks might have experienced two or three events of hydrocarbon generation since the Triassic, which could be caused by multiphase tectonic movements from the Indosinian to the Himalayan. Residual coaly source rocks buried deeper than 4000 m and experienced high thermal evolution. These source rocks provided lots of petroleum and gas with maturity ranging from 0.76 to 2.50% R_o (Chang et al., 2018). Although these coaly source rocks are extensively investigated, the differences in their hydrocarbon potential and the relationship between condensate and coaly source rocks remain unclear. C–P coaly source rocks can be further divided into five lithotypes of clarain, durain, carbonaceous shale, deltaic shale, and lagoonal shale according to their maceral components and depositional environments. Most coals were observed to be semi-clarain–semi-durain, which were divided into durain and clarain according to the types and contents of maceral components. The shales of the Shanxi and Taiyuan formations can be classified into deltaic shale deposited in delta plain and frontier environments and lagoonal shale formed in lagoon environments, respectively. However, the differences in the hydrocarbon potential of the five types of coaly source rocks have rarely been discussed. Moreover, there are no controlled parameters for clarifying the differences among coaly source rocks and coaly-related oils, which can account for the effect of similar maceral components of coaly source rocks. Therefore, the complexity of lithologies enhances the identification difficulty of the relative generation relationship from coaly source rock to coaly-related oils.

This study aimed to outline the organic geochemical differences among coaly source rocks (clarain, durain, and coaly shales of carbonaceous shale, deltaic shale, lagoonal shale) and coaly-related oils, and develop more accurate parameters to explore the evident discrepancies among the five types of coaly source rocks. New and effective parameters are expected to attain and clarify different lithologies of coaly source rocks. Therefore, the hydrocarbon generation processes and oils generated from five types of coaly source rocks were investigated through organic geochemical analysis and thermal simulation. This study provides new insights to judge the linkage between coaly-related oils and coaly source rocks. And the approach could be useful for studying source rocks deposited in similar environments worldwide.

2 Geological background

The Bohai Bay Basin formed above the North China Craton and developed from Mesozoic to Cenozoic (Li et al., 2015; Zhao et al., 2018). The Huanghua depression is located in the northwestern part of the Bohai Bay Basin and contains abundant petroleum resources (Fig. 1(a); Zhou et al., 2012. The succession of Upper Paleozoic contains the Benxi, Shanxi, Taiyuan, and Shihezi Formations (Fig. 1(c)), which developed thick (178–369 m), unconformable, siliciclastic-led deposits. Above the Middle Ordovician carbonates, the strata were formed in shallow-marine and paralic environments (Kim, 2001).

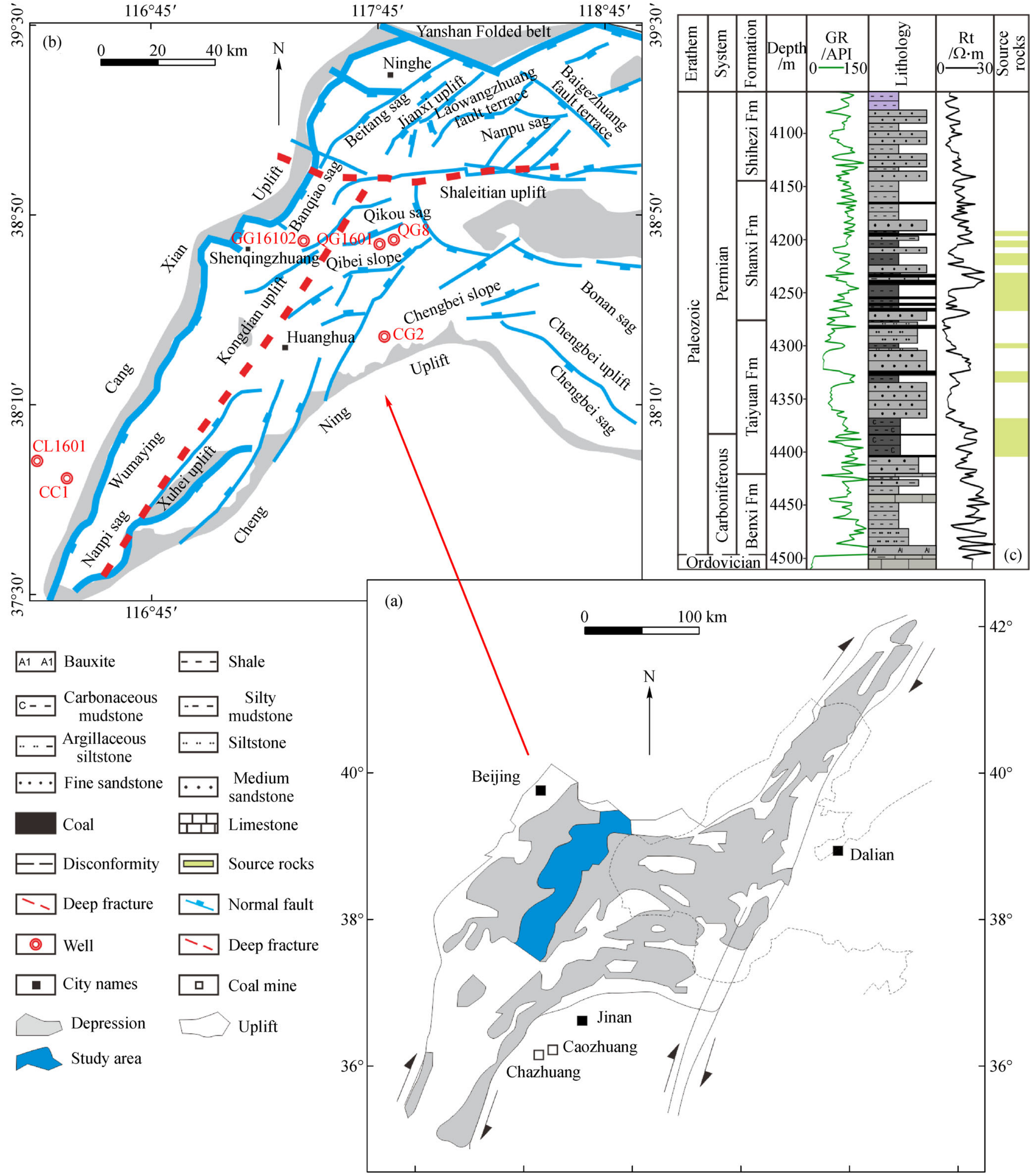

Fig. 1 Study area and coaly source rock profile of the Carboniferous–Permian in the Bohai Bay Basin. (a) Bohai Basin; (b) research area; (c) stratigraphic sequence.

The Shanxi and Taiyuan formations accumulated coaly source rocks in the paralic environments from late Carboniferous to early Permian (Liu, 1990), and showed commercial coaly-related hydrocarbons (Fig. 1; Lv and Chen, 2014; Zhao et al., 2018). The coaly source rocks comprise of coal, carbonaceous mudstone and dark mudstone. As brightness and thickness decrease, the lithology of the coal samples changes from clarain to durain and deposited in the lagoon and delta environments. Carbonaceous mudstone was identified by high peat content and predominanted by argillaceous minerals and larger fossilized plant stems. The composition of the mudstone was controlled by its depositional environment, including salinity, hydrodynamic conditions, and organic matter input caused by the shift from lagoonal to prodeltaic environments. Accordingly, the mudstone can be divided into lagoonal shale and deltaic shale (Xu and Jin, 2020). The coaly source rocks happened primary hydrocarbon generation during the mid-Triassic (T), which induced by regional tectonic settlement and terminated by uplift from the late T; A rift basin formed in east China during the Jurassic (J) to Cretaceous (K), and some coaly source rock generated hydrocarbons for the second time (early-secondary hydrocarbon generation); since the Eocene, a new rift basin developed on residual J–K strata, with some of the coaly source rocks buried deep beneath the sag areas of the rift generating oil and gas for a second (late-secondary hydrocarbon generation) or third time (tertiary hydrocarbon generation) (Xu and Jin, 2020).

3 Materials and methods

3.1 Samples

A total of 36 coaly source rock samples were selected from wells CG2, CC1, GG16102, QG1601, QG8, and CL1601, as well as Caozhuang and Chazhuang coal mines in the Feicheng. Furthermore, five samples including clarain, durain, carbonaceous shale, lagoonal shale, and deltaic shale, were selected to conduct the thermal simulation experiment (Table 1). The oils and gas samples gathered from the thermal simulation experiments were analyzed for the biomarker analysis.

3.2 Analytical methods

3.2.1 Total organic carbon and Rock-Eval pyrolysis

Two hundred milligrams of the crushed samples (~200 mesh) were weighed to acidate with HCl at 60°C and wash with distilled water in a crucible. After the carbonate contents were removed, the washed subsamples were subsequently dried for 24 h at 50°C. TOC contents were measured with a LECO CS–230 analyzer. The Rock-Eval pyrolysis was analyzed with an OGE-II instrument with 60 to one hundred grams of each crushed sample. The crushed samples were placed in a helium atmosphere for heating. The heating procedure was set at a rate of 50°C/min and the temperature increased from 300°C to 600°C.

3.2.2 Maceral components analysis

Samples were polished and performed at the organic geochemistry laboratory of the China University of Petroleum (East China) following ISO procedures (ISO 7404-2, 2009). The component observation of organic petrology and determination of vitrinite reflectance were carried following standard procedures (ISO7404-3, ISO7404-5, 2009) under reflected light conditions of white and blue light excitation, following the ICCP System 1994 nomenclature (ICCP, 1998, 2001; Pickel et al., 2017). The samples were observed under an ultraviolet (UV) fluorescence microscope (Zeiss Axio Scope A1 POL) with magnifications at 200×, 500×, and 1000×.

3.2.3 Thermal simulation experiments

The thermal simulator can resist high temperatures and high pressures separately, up to 800°C and 120 MPa. The crushed samples (~100 mesh) are closed in the autoclave accompanying nitrogen or distilled water (adding as 25% of sample mass) and heated by a heater strip at a set heating rate. With a heating rate of 60°C/h, all coal samples were heated from 300°C to 650°C directly with every 50°C intervals. Every temperature point of a total of 6 points needs a 5 to 7 g of samples. The liquid products are dissolved through solvent dichloromethane (DCM) and analyzed by Gas chromatography-mass spectrometry (GC–MS) analyzer.

3.2.4 Gas chromatography-mass spectrometry (GC–MS) analysis

For GC–MS analysis, soxhlet extraction was used to treat the powdered samples for 72 h with dichloromethane. Asphaltenes solved in a mixture solution of hexane-DCM (80:1) were removed by centrifugal separation. The hydrocarbons and NSO compounds were separated with column chromatography (filled with silica gel and Al_2O_3). In which, the saturates were eluted with hexane, and the aromatics were extracted with DCM-hexane solution (2:1). The saturated and aromatic hydrocarbons were measured by a gas chromatograph coupled to an Agilent 7890 GC–MS. The fused silica column in the GC-MS analyzer was 30 m DB-5MS (i.d. 0.25 mm; 0.25 μm film thickness). The oven was heated from 70°C to 300°C at a rate of 3°C/min and lasted constant temperature for 30 min. The scan range of the mass-to-charge ratio was set from 50 to 650 with a total scan time of 0.7 s. Every compound was analyzed following the NIST library and the published data of mass spectra.

4 Results

4.1 Bulk geochemical parameters

Organic matter abundance showed a clear downward trend from coal to shale samples (Fig. 2). The total organic carbon content (TOC) of durain and clarain samples was higher than that of other samples, ranging from 50.6 wt% to 71 wt%. TOC values of carbonaceous shale ranged from 7.58 wt% to 24.80 wt%. Deltaic and lagoonal shales presented relatively lower TOC content (1.27–7.68 wt%; Fig. 2(a)). The S_2 (0.90–236.57 mg/g)values of all samples showed roughly the same trend with TOC content (Table 1). Compared to the diagram of S_1 versus TOC

Table 1 Organic geochemical parameters of coaly source rocks

Samples	Well/area	Formation	Lithology	Depth/m	TOC/ wt%	S_1/ $(mg\cdot g^{-1})$	S_2/ $(mg\cdot g^{-1})$	$S_1 + S_2$/ $(mg\cdot g^{-1})$	T_{max}/ °C	HI/ $(mg\cdot g^{-1}\cdot TOC^{-1})$
C1	Caozhuang	Shanxi	Clarain#	350.00	71.00	1.32	167.78	169.10	432	236.31
C2	CG2	Taiyuan	Clarain	1690.63	68.10	3.84	208.70	212.54	434	306.46
C3	CG2	Taiyuan	Clarain	1598.13	67.90	2.18	154.03	156.21	438	226.85
C4	GG16102	Taiyuan	Clarain	2224.55	70.10	2.17	154.19	156.36	432	219.96
C5	CL1601	Taiyuan	Clarain	2276.11	65.70	10.61	160.81	171.42	457	244.76
C6	Chazhaung	Shanxi	Clarain	300.00	57.00	4.76	195.97	200.73	437	343.81
C7	Chazhaung	Shanxi	Clarain	420.00	54.60	8.36	228.21	236.57	431	417.97
D1	Chazhaung	Shanxi	Durain	450.00	50.60	2.89	138.03	140.92	431	272.79
D2	Chazhaung	Taiyuan	Durain	780.00	61.20	2.27	158.02	160.29	436	258.20
D3	Caozhuang	Taiyuan	Durain#	750.00	56.50	1.11	119.35	120.46	432	211.24
D4	CG2	Taiyuan	Durain	1690.63	40.00	0.95	49.61	50.56	438	124.03
D5	GG16102	Taiyuan	Durain	2224.55	69.40	2.30	91.23	93.53	431	131.46
CS1	Chazhaung	Taiyuan	Carbonaceous shale	635.00	14.70	2.13	49.80	51.93	441	338.78
CS2	QG8	Taiyuan	Carbonaceous shale	3704.00	22.93	3.66	51.23	54.89	437	223.42
CS3	QG1601	Taiyuan	Carbonaceous shale	3879.00	23.90	1.92	39.18	41.10	444	163.93
CS4	QG1601	Taiyuan	Carbonaceous shale	3801.00	37.40	5.07	87.03	92.10	443	232.70
CS5	QG1601	Shanxi	Carbonaceous shale	3750.00	26.10	3.11	87.60	90.71	443	335.63
CS6	GG16102	Taiyuan	Carbonaceous shale	2198.09	27.77	3.70	57.02	60.71	430	205.31
CS7	GG16102	Taiyuan	Carbonaceous shale	2211.78	22.03	1.79	44.30	46.09	428	201.09
CS8	QG8	Taiyuan	Carbonaceous shale	3710.00	13.13	1.15	12.89	14.04	441	98.17
CS9	QG1601	Taiyuan	Carbonaceous shale	3717.00	15.50	1.69	38.13	39.82	438	246.00
CS10	QG1601	Taiyuan	Carbonaceous shale	3819.00	17.10	2.12	37.92	40.04	440	221.75
CS11	CG2	Taiyuan	Carbonaceous shale#	1602.95	7.58	0.44	21.00	21.44	436	277.04
CS12	CL1601	Taiyuan	Carbonaceous shale	2273.20	11.50	1.82	10.19	12.01	469	88.61
CS13	CL1601	Taiyuan	Carbonaceous shale	2270.95	24.80	4.27	78.80	53.07	464	317.74
CS14	CL1601	Taiyuan	Carbonaceous shale	2101.79	17.60	0.97	15.64	16.61	457	88.86
DS1	Chazhaung	Shanxi	Deltaic shale	350.00	6.07	0.10	14.14	14.24	435	232.95
DS2	CC1	Shanxi	Deltaic shale	1593.59	4.38	0.18	1.03	1.21	476	23.52
DS3	CC1	Shanxi	Deltaic shale	1594.25	7.68	0.56	2.90	3.46	480	37.76
DS4	CG2	Shanxi	Deltaic shale#	1587.88	1.92	0.07	1.63	1.7	440	84.90
LS1	Chazhaung	Taiyuan	Lagoonal shale	760.00	5.62	0.37	6.54	6.91	440	116.37
LS2	Chazhaung	Taiyuan	Lagoonal shale#	780.00	5.75	0.10	1.86	1.96	452	32.35
LS3	CL1601	Taiyuan	Lagoonal shale	2279.91	2.38	0.32	1.49	1.81	473	62.61
LS4	CL1601	Taiyuan	Lagoonal shale	2275.91	2.33	0.23	1.19	1.42	469	51.07
LS5	CL1601	Taiyuan	Lagoonal shale	2259.09	3.27	0.22	2.64	2.86	463	80.73
LS6	CL1601	Taiyuan	Lagoonal shale	2256.97	1.27	0.15	0.75	0.90	464	59.06

Note: #, Thermal simulation samples.

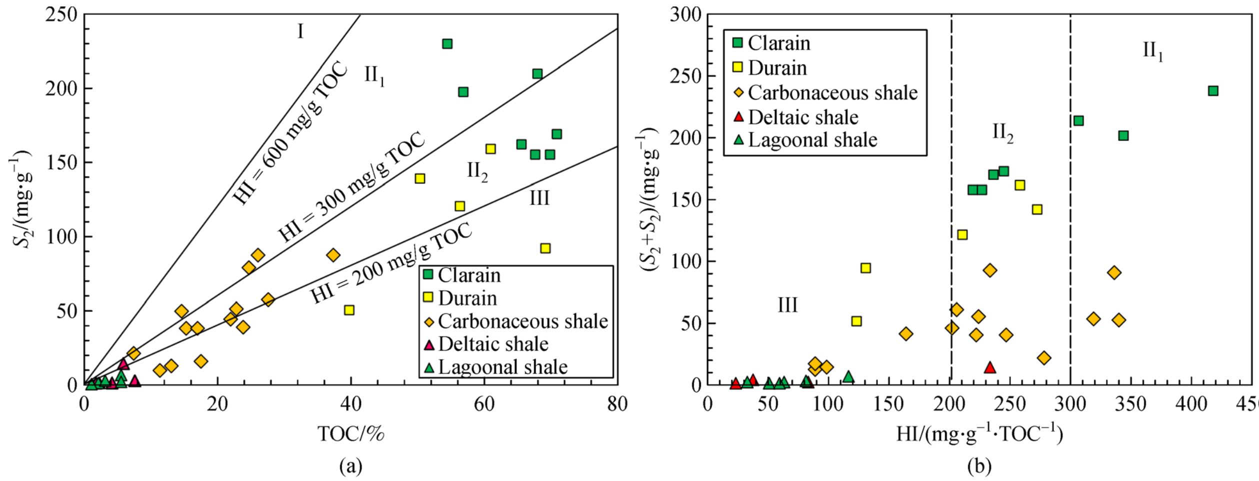

Fig. 2 Organic matter abundance and maceral compositions of coaly source rocks (modified from Peters and Cassa, 1994).

values, hydrocarbon potential ($S_1 + S_2$) and hydrogen index (HI) presented a transition area among five coaly source rocks (Fig. 2(b)). Clarain samples exhibited higher $S_1 + S_2$ (156.21–212.54 mg/g) and HI (TOC of 219.96–306.46 mg/g). Although durain samples also had high $S_1 + S_2$, their HI was low compared to carbonaceous shale. Lagoonal shale samples showed lower TOC and higher HI values, whereas deltaic shale samples exhibited the opposite trend (Figs. 2(a) and 2(b)). All Rock-Eval pyrolysis parameters exhibited a distinct difference in kerogen types from clarain to lagoonal shale samples. The vast majority of clarain samples falls under the type II_2 area, except for one sample (type II_1). The durain and carbonaceous shales corresponded to type II_2 to type III, while deltaic and lagoonal shales were characterized by type III.

4.2 Organic petrology

Apparent differences presented in maceral components and contents among five coaly source rocks (Fig. 3). As shown in Table 2, coal samples were mainly composed of vitrinite. More than 80% of hydrogen-rich collodetrinite in clarain are present in the matrix as indicated by dark green fluorescence (Fig. 3(a)). Furthermore, sporinites and cutinites occur as bedding laminations within hydrogen-rich collodetrinite (Figs. 3(a) and 3(b)). In contrast, durain and carbonaceous shale contain more hydrogen-poor collotelinite and black corpogelinite with slight sporinites instead of hydrogen-rich collodetrinite (Figs. 3(c) and 3(d)). A significant decrease in vitrinite content was observed in deltaic and lagoonal shale samples (Figs. 3(e) and 3(f)). In addition, small amounts of cutinites and sporinites were presented in shales.

The type and content of maceral components exhibited some correlations with TOC content. TOC contents present a positive correlation with vitrinite content, and poor relationship with liptinite content (Fig. 4(a)). Statistics showed high contents of hydrogen-rich collodetrinite in the clarain (> 45%) and durain (average 52.57%) samples, except for one sample (Fig. 4(b); Table 2). However, the vitrinite content of durain samples was extremely low, and TOC content was strongly associated with liptinite (Table 2). The contents of hydrogen-poor vitrinite and liptinite in carbonaceous shale show poor correlated to TOC content, which contents of liptinite ranging from 2.1% to 10.5% (Table 2). Despite the low content of maceral components, the deltaic and lagoonal shale samples exhibited an obviously increasing trend between hydrogen-poor vitrinite and TOC contents (Fig. 4(b)). Nevertheless, no relationship was between liptinite and TOC contents (Fig. 4(a)).

4.3 Hydrocarbon generation processes of coal and coaly shale

In the thermal simulation of the five types of source rocks, different hydrocarbon generation processes were observed during their evolution. Except for carbonaceous shale and lagoonal shale, the yield of liquid hydrocarbons peaked at 450°C. The yield of liquid hydrocarbons in carbonaceous shale began to peak at 400°C, whereas that in lagoonal shale peaked at approximately 525°C, showing a delay of more than 70°C (Fig. 5(a)). Before the peaking of liquid hydrocarbon generation, five types of source rocks exhibited significant differences in yield. Carbonaceous shale maintained a high yield until the peak at around 26.58 mg/g TOC. Before the temperature of 375°C, the durain had a higher yield than clarain and shales. For each sample, there was no clear difference in yield after the peak, with a decreasing trend till the end limit of the simulation.

Regarding the gas hydrocarbon generation process, all samples featured a similar increasing trend (Fig. 5(b)).

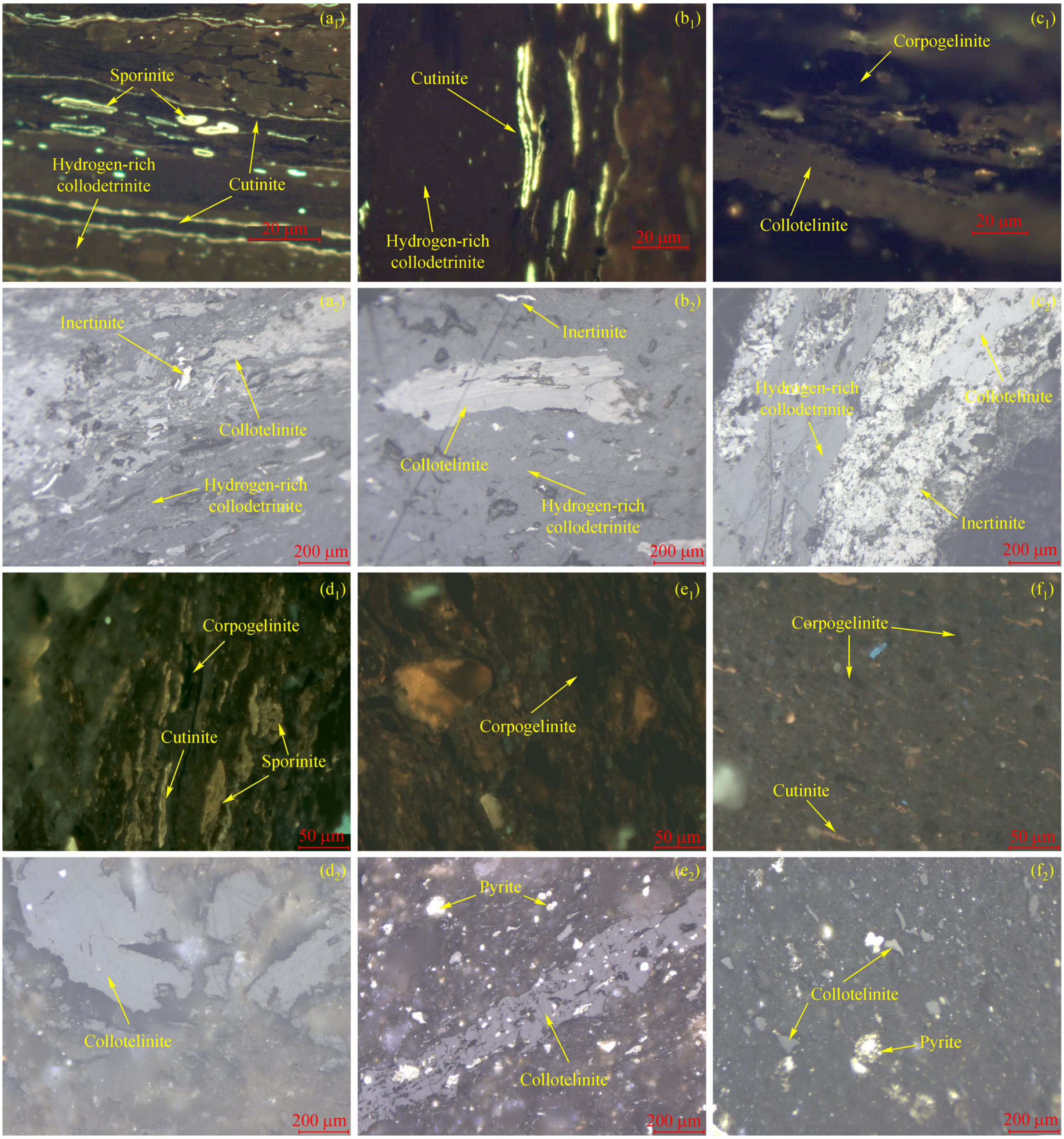

Fig. 3 Maceral components accumulated in coaly source rocks. (a_1), (b_1) abundant green-yellow hydrogen-rich collodetrinite, sporinite and cutinite, reflecting fluorescent light under UV conditions; and white light, clarain (C6), Shanxi Formation, 1000×, 500×; (a_2), (b_2) dark gey collodetrinite, light gray collotelinite, off-white inertinite, clarain (C6), Shanxi Formation, 200×, 200×; (c_1), (c_2) larger fuscous collotelinite and black corpogelinite under UV conditions, dark gey collodetrinite, light gray collotelinite, and off-white inertinite under white light condition, durain (D1), Shanxi Formation, 500×, 200×; (d_1), (d_2) yellow sporinite with an apparent cell and black corpogelinite under UV conditions, light gray collotelinite under white light condition, carbonaceous shale (CS11), Taiyuan Formation, 500×, 200×; (e_1), (e_2) black corpogelinite under UV conditions, light gray collotelinite and bright white pyrite under white light condition, deltaic shale (DS3), Shanxi Formation, 500× , 200×; (f_1), (f_2) shallow yellow cutinite and black corpogelinite under UV conditions, a few light gray collotelinite and bright white pyrite under white light condition, lagoonal shale (LS5), Taiyuan Formation, 500×, 200×.

Table 2 Organic geochemical parameters and maceral components of coaly source rocks

Samples	Well/area	Formation	Lithology	Depth/m	R_o/%	TOC/%	$(S_1 + S_2)$/$(mg \cdot g^{-1})$	T_{max}/°C	Liptinite/%	Vitrinite/%		Inertinite/%	Bituminite/%
										Hydrogen-poor	Hydrogen-rich		
C5	CL1601	Taiyuan	Clarain	2276.11	1.00	65.7	171.42	457		21.5	59.0	9.4	1.8
C6	CHZ-7	Shanxi	Clarain	300.00	0.65	57.0	200.73	437	3.1	47.6	32.5	11.2	
C7	CHZ-5	Shanxi	Clarain	420.00	0.67	54.6	236.57	431	3.9	88.6	1.2	0	
D1	CHZ-11	Shanxi	Durain	450.00	0.65	50.6	140.92	431	28.3	22.0	8.3	36.2	
CS1	CZ-9	Taiyuan	Carbonaceous shale	635.00	0.66	14.7	51.93	434	5.6	48.4		4.3	3.7
CS11	CG2	Taiyuan	Carbonaceous shale	1602.95	0.64	7.58	21.44	436	10.5	24.5		26.8	0.1
CS12	CL1601	Taiyuan	Carbonaceous shale	2273.2	0.92	11.5	12.01	469	6.5	6.2		0.2	8.0
CS14	CL1601	Taiyuan	Carbonaceous shale	2101.79	0.92	17.6	16.61	457	2.1	8.4		45.6	0.1
DS2	CC1	Shanxi	Deltaic shale	1593.59	1.15	4.38	1.21	476	0.7	7.4		0.1	10.1
DS3	CC1	Shanxi	Deltaic shale	1594.25	1.14	7.68	3.46	480		13.6		0.1	9.8
LS3	CL1601	Taiyuan	Lagoonal shale	2279.91	1.02	2.38	1.81	473		2.6			1.4
LS2	CHZ-4	Taiyuan	Lagoonal shale	780.00	0.65	5.75	1.96	452	1.5	4.2		0.2	1.3
LS4	CL1601	Taiyuan	Lagoonal shale	2275.91	1.00	2.33	1.42	469		2.2		0.1	2.7
LS5	CL1601	Taiyuan	Lagoonal shale	2259.09	0.96	3.27	2.86	463	2.1	3.4		0.2	9.4
LS6	CL1601	Taiyuan	Lagoonal shale	2256.97	1.07	1.27	0.9	464	0.8	1.4			6.0

Notes: Liptinite including alginite and exinite of sporinite, cutintie, resinite. Vitrinite including hydrogen-poor components of telinite, gelinite, and vitrodetrinite and hydrogen-rich of colotellinite, corpogelinite, and collodetrinite. Bituminite including secondary asphalt and mineral pithch.

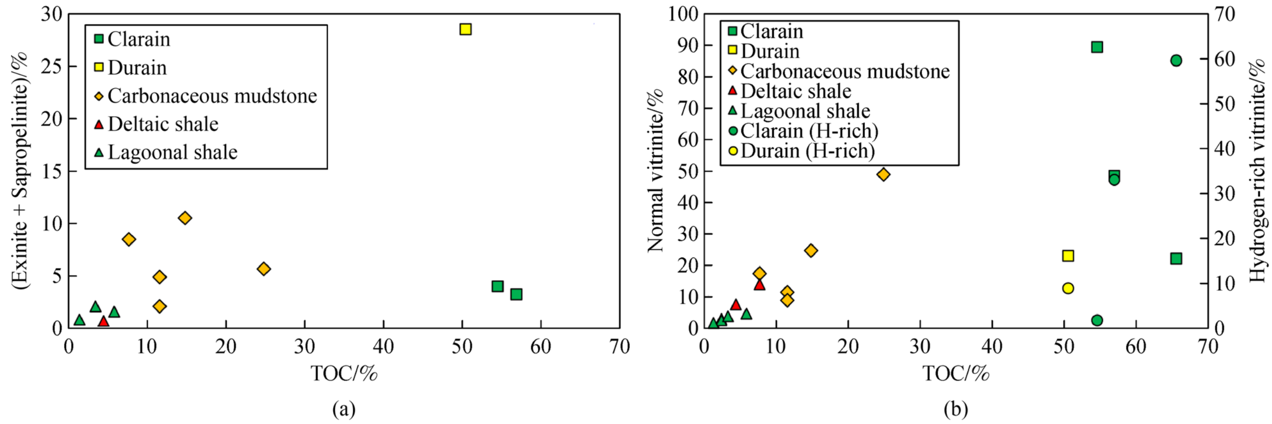

Fig. 4 Plots of liptinite, hydrogen-poor vitrinite, hydrogen-rich vitrinite vs. total organic carbon (TOC) within coaly source rocks.

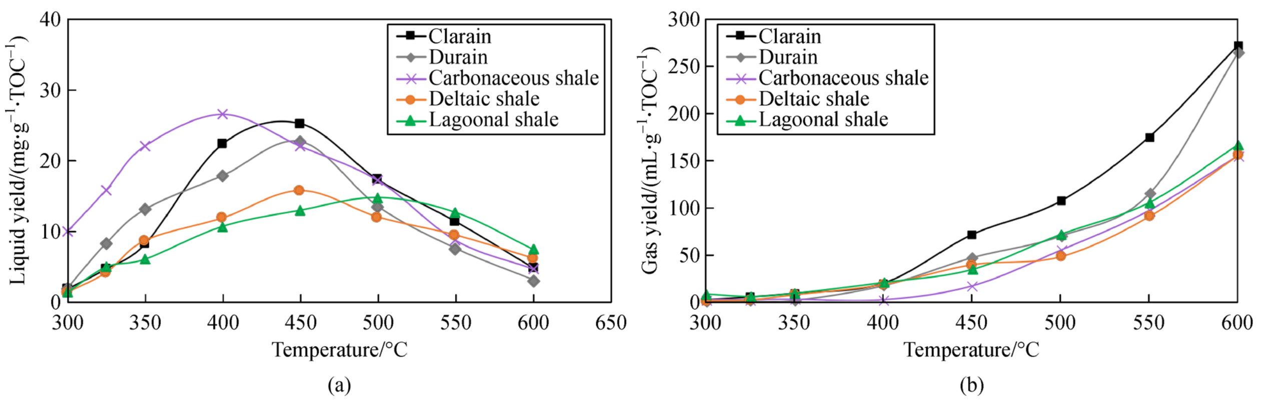

Fig. 5 Processes and yields of liquid and gas hydrocarbon generation changing in the thermal simulation.

After reaching the temperature of 400°C, striking differences began to appear, and clarain exhibited a significant increase in gas hydrocarbon generation, accounting for the highest gas yield. Deltaic and carbonaceous shales presented the lowest gas yield before 600°C. Finally, durain samples exhibited a sharp increase of gas hydrocarbon yield at 550°C and the yield approached that of the clarain sample (Fig. 5(b)).

4.4 Changes in saturated hydrocarbons and aromatic compounds during hydrocarbon generation

With increasing temperature, the five types of source rocks exhibited apparent differences in the evolution of saturated hydrocarbons and aromatic compounds (Fig. 6, Fig. 7, and Fig. 8). The clarain and durain samples showed relatively high and stable ratios of pristane and phytane (Pr/Ph), and other samples presented no obvious regularity (Fig. 7(a)). Similar characteristics were observed for the ratios of lower ($\sum nC_{21-}$) and higher normal alkanes ($\sum nC_{22+}$) in coaly source rocks, showing no strong discriminative power (Fig. 7(b)). Compared to the evolution of isoparaffin and normal alkanes, hopane and sterane series compound displayed distinct differences before reaching the temperature of 550°C (Figs. 7(c) and 6(d)). With increasing temperature, the carbonaceous shale, clarain, and durain samples exhibited increasing trends of Ts/(Ts + Tm), Ga/C_{30} hopane, and C_{27} steranes/C_{29} steranes (Fig. 6). However, these parameters remained relatively stable in lagoonal and deltaic shales with slight fluctuations and values higher than those of other samples. The ratios of Ga/C_{30} hopane and Oleanane/C_{30} hopane in lagoonal shales were different from those of other samples (Figs. 6(c), 7(d) and 7(f)).

The saturated hydrocarbons, such as phenanthrene, fluorene, and naphthalene compounds, showed various evolution trends as increasing temperature (Figs. 6 and 7). Except for parameter MPI2, all samples can be identified according to the evolutionary character of the DBF/F ratio, DBT/F ratio, and MNR (Figs. 8(a), 7(b) and 7(d)). Lagoonal and carbonaceous shales exhibited higher values (>1.0) and a fluctuant trend of DBT/F ratio above the smooth trend of durain, deltaic shale, and clarain (Figs. 6 and 8(b)). Similar evolutional trends of DBF/F ratio and MNR were observed in all samples with a reversed order of parameters (Figs. 8(a) and 7(d)). After the temperature of

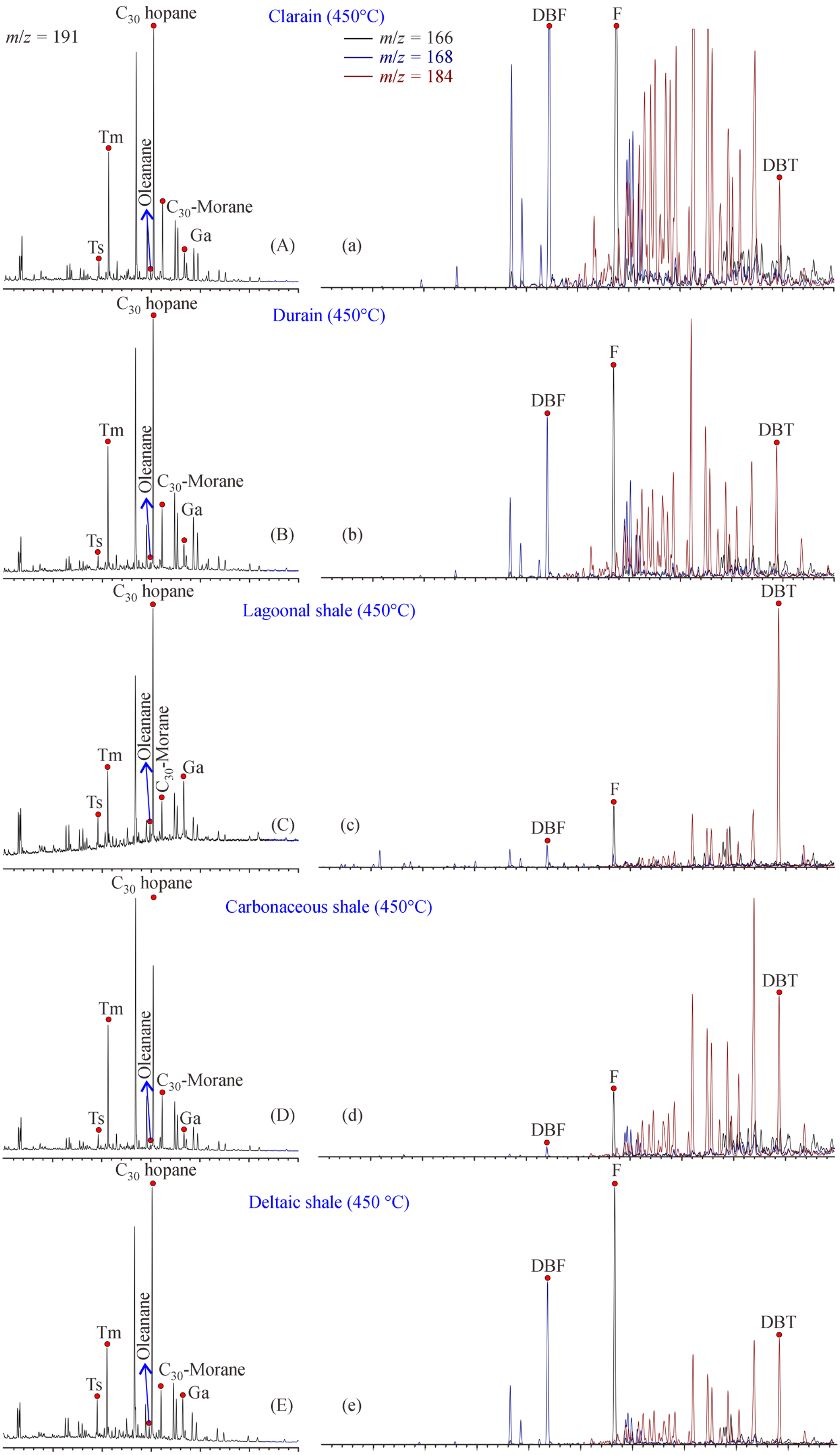

Fig. 6 Chromatography of hopane series (m/z = 191) and fluorene series (m/z = 166, 168, 184) compounds. Ts: 18α(H)-22,29,30-C_{27} hopane; Tm: 17α(H)-22,29,30-C_{27} hopane; Ga: Gammacerane (γ-C_{30} hopane); F: fluorene; DBF: dibenzofuran; DBT dibenzothiophene.

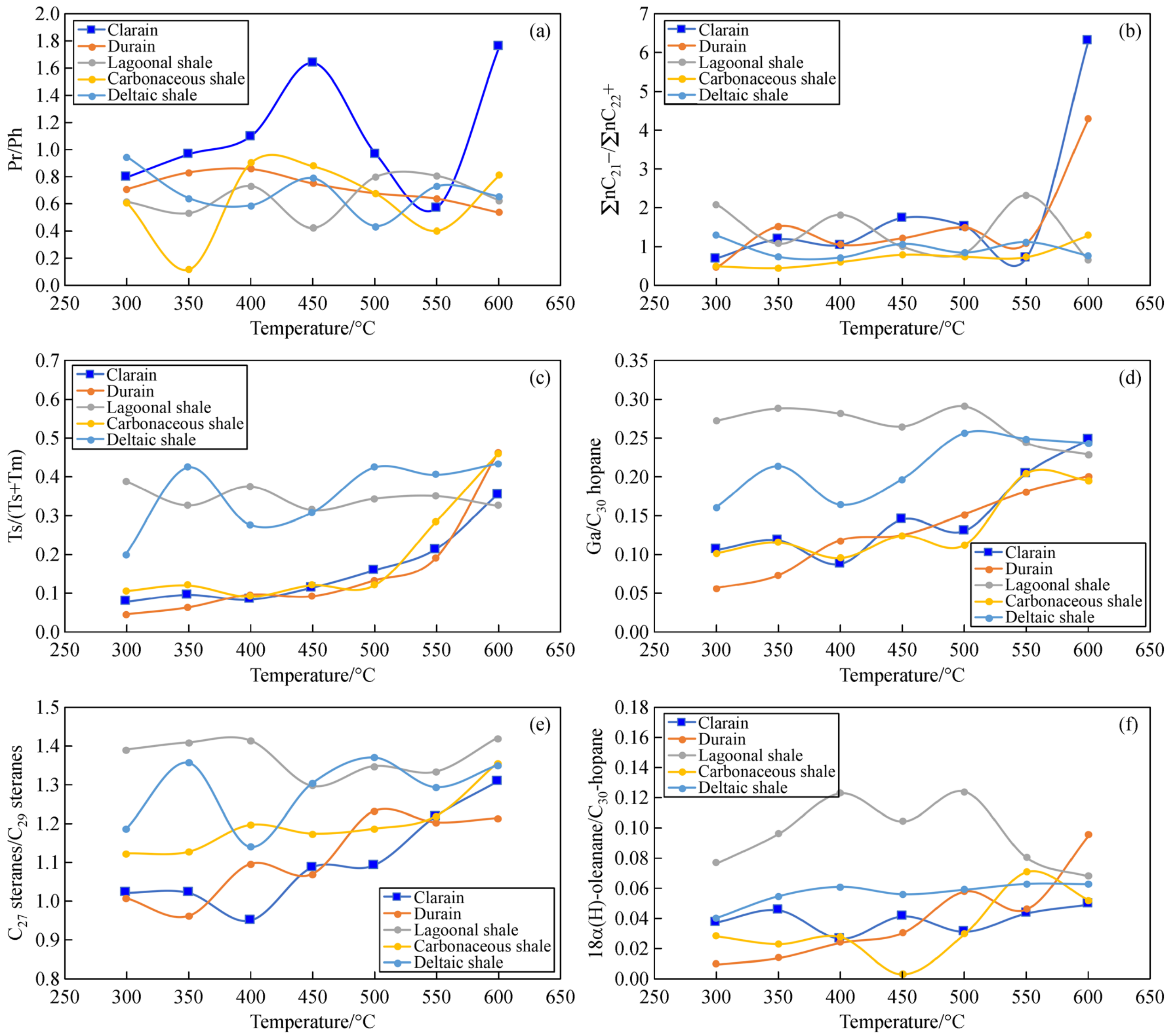

Fig. 7 Variations in saturated hydrocarbon parameters in the thermal simulation. Pr: pristane; Ph: phytane.

400°C, MPI2 values as increasing temperature decreased in lagoonal and deltaic shale and increased in coal and carbonaceous shale (Fig. 8(c)).

5 Discussion

5.1 Differences in hydrocarbon generation potential

Regarding C-P coaly source rocks deposited in a paralic environment, the hydrocarbon potential is closely related to types and contents of maceral components (e.g., hydrogen-rich collodetrinite, alginite, resinite, and sporinite; Stasiuk, 1994; Petersen et al., 2000; Tewari and Khan, 2015). According to the results of TOC and Rock-Eval tests, clarain and durain have the highest potential to generate hydrocarbons, with values of $S_1 + S_2$ ranging from 236.57 mg/g to 140.92 mg/g (Fig. 2; Table 2). In contrast, lagoonal and deltaic shales have the lowest potential with values of $S_1 + S_2$ ranging from 3.46 mg/g to 0.90 mg/g. The hydrocarbon generation potential of carbonaceous shale lies between those of coals and dark shales with an average $S_1 + S_2$ of 45.33 mg/g. Observations of the maceral composition revealed that clarain contains more normal and H-rich vitrinites, showing a positive relationship with TOC content instead of liptinites of sporinite and cutinite (Figs. 3 and 4; Table 2). The durain contains more collotelinite and corpogelinite with a higher proportion of short-chain aliphatic and aromatic carbon compounds and liptinite with more long-chain aliphatic carbon compounds than the clarain (Fig. 3; Table 2). The liptinite is believed to agree well with hydrocarbon generation than the vitrinite (Fig. 4). The maceral compositions of coal samples mainly

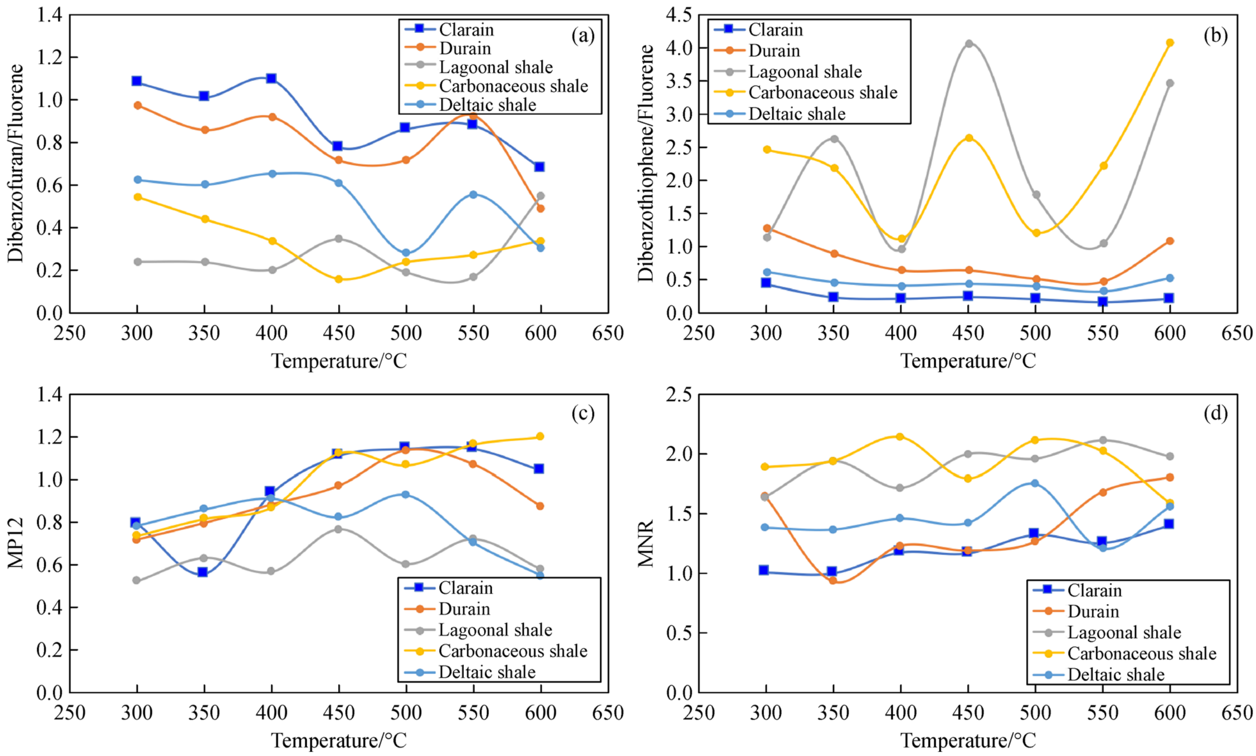

Fig. 8 Variations in phenanthrene, fluorene, and naphthalene compounds in the thermal simulation. MPI2 = 3 × 2-methylphenanthrene/(Methylphenanthrene + 1-methyphenanthrene + 9-methylphenanthrene); MNR = 2-methylnaphthalene/1-methylnapthalene.

originated from terrigenous woody and herbaceous plants rather than algae (Petersen et al., 2000; Tewari and Khan, 2015).

The clarain deposited in a reducing low-stand swamp environment and accumulated more hydrogen-rich collodetrinite which is gelled with exinite of cutinite and sporinite (Hartgers et al., 1994; Tewari and Khan, 2015; Li et al., 2019a, 2019b). Due to strong biodegradation and gelatinization, more hydrogen-rich sporinite, resinite, and cutinite were cemented into collodetrinite (Figs. 3(a) and 3 (b)). Therefore, the hydrogen-rich collodetrinite is considered to be the main contribution to the high hydrocarbon potential of the clarain. During a deposition in the weak reduction and hydrodynamic fluctuation environment, the durain contained more terrestrial detrital input (Tewari and Khan, 2015). The collotelinite and corpogelinite in durain occurred as hydrogen-poor uniform gels due to simple gelatinization kinetics (Petersen et al., 2000; Suwarna, 2006; Li et al., 2019b). The hydrocarbon generation of the durain showed a decreasing trend (Fig. 2). The carbonaceous shale was formed in more oxygen environments (e.g. shallow water swamps or upland moors) with plentiful terrigenous plants input (Greb and Martino, 2005; Li et al., 2019a, 2019b), comprising argillaceous minerals and coaly debris characterized by hydrogen-poor vitrinite. These conditions explain the low petroleum potential of the carbonaceous shale. The lagoonal shale developed in the lagoonal environment of the Taiyuan Formation and accumulated hydrogen-poor vitrinite and little bituminous organic matter, showing the lowest hydrocarbon potential (Fig. 3; Li et al., 2019a). Under the influence of marine regression, more vitrinite, sporinite, and cutinite were accumulated in the deltaic shale than lagoonal shale during deposition of the Shanxi Formation, which is indicated by higher hydrocarbon-rich macerals (Fig. 3). Terrigenous organic matter, such liptinite, hydrogen-rich, and hydrogen-poor vitrinite, controlled the hydrocarbon generation of five types of coaly source rocks.

5.2 Implications for distinguishing lithologies of five types of coaly source rocks

Although saturated and aromatic fractions were the main components of organic matter in the coaly source rocks, the proportion of different compounds varied significantly, which was revealed by biomarker analysis at every temperature.

The relative contents of different isoprenoid, sterane, and terpane compounds were used to classify the marine and lacustrine environments. The evaporitic, deltaic, and carbonate environments were further identified from marine with above parameters. For instance, pristane/phytane ratios and short-chain versus long-chain normal alkanes ($\sum nC_{21-}/\sum nC_{22+}$) were used to identify the coal and shales deposits in swamps and paleolakes, respectively (Mello et al., 1988; Hughes et al., 1995). However, the evolution of above parameters presented minor differences among coal, carbonaceous shale, and dark shale from a paralic environment (Figs. 7(a) and 7(b)). In the thermal simulation, discrepancies were observed in the evolution of Ts/(Ts + Tm), Ga/17α(H)21β(H)-C_{30} hopane, 18α(H)-oleanane/17α(H)21β(H)-C_{30} hopane, and 17β(H)21α(H)-C_{30} morane/17α(H)21β(H)-C_{30} hopane between coal, carbonaceous shale, and dark shales. These discrepancies are considered a good indicator for differentiating coal/carbonaceous shale and dark shales. Dark shales were characterized by high ratios of Ts/(Ts + Tm) (>0.20), Ga/17α(H)21β(H)-C_{30} hopane (>0.15), and 18α(H)-oleanane/17α(H)21β(H)-C_{30} hopane (>0.05), and low ratios of 17β(H)21α(H)-C_{30} morane/17α(H)21β(H)-C_{30} hopane (<0.25), in contrast to those of coal and carbonaceous shale (Fig. 9).

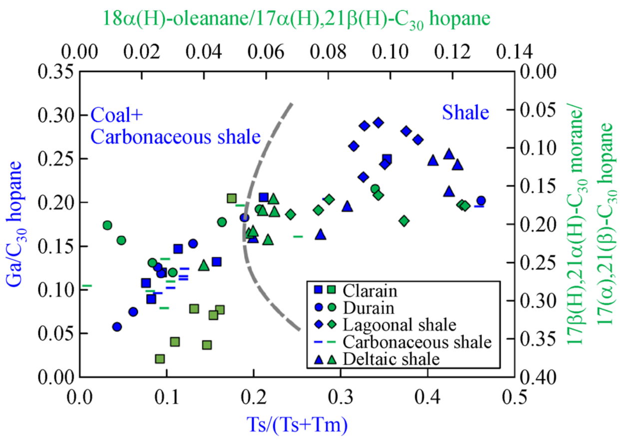

Fig. 9 Parameters of hopane series compounds for lithology identification from thermal simulation.

Aromatic series compounds bear useful implications for the depositional environments, source input, and maturity of organic matter in the clarain, durain, lagoonal shale, and deltaic shale (Luo et al., 2001; Wei et al., 2001; Li et al., 2001). The naphthalene, phenanthrene, and fluorene series of the aromatic fraction presented different characteristics within coaly source rocks (Fig. 8).

The abundant DBT accumulated in old organic-rich deposits is thought of as a consequence of a catalytic reaction between biphenyl ring systems and surface-adsorbed sulfur on carbonaceous material (Asif et al., 2009; Asif, 2010). DBFs trended to accumulate in source rocks deposited in fresh water and terrigenous oils and coals (Li et al., 2004; Li et al., 2013). The parameters of DBT/P ratio and Pr/Ph ratios in crude oils were useful for identifying the sedimentary environment and different lithotypes (Hughes et al., 1995). However, the application of this plot was found to be unsuitable for source rocks deposited in paralic and lacustrine/swamp environments (Radke et al., 2000). Due to variable sedimentary environments and similar source of organic matter, the discrimination for different lithologies of coaly source rocks was difficult to be identified. As mentioned in the literature review, the concentrations of naphthalene and methyl-substituted naphthalene series compounds were closely related to terrigenous organic matter input (Radke and Willsch, 1994). Further investigation on the Permian coal of the southern Sydney Basin revealed that coal/coaly shales possess lower MNR and DBT/P ratio, and similar TeMNR compared to fine-grained sediments (Ahmed et al., 2009).

Integrating the information of the sedimentary environment and source input, and results of the thermal simulation experiment, five types of C–P coaly source rocks could be well distinguished by several parameters of the aromatic fraction (e.g., TeMNR, MNR, DBT/F ratio, DBF/F ratio). In terms of TeMNR versus MNR, the carbonaceous shale is characterized by low TeMNR (<0.40) and high MNR (>1.80), and a depositional zone close to the lagoonal shale facies. In contrast, the durain is characterized by higher TeMNR (>0.56) and lower MNR (<1.80) (Fig. 10(a)). Lagoonal shale, deltaic shale, and clarain have similar TeMNR values and lie between carbonaceous shale and durain with moderate TeMNR and MNR. In different lithologies, the MNR varied in the descending order of lagoonal shale > deltaic shale > clarain (Fig. 10(a)). Significant differences were found between naphthalene and fluorene series compounds. The clarain and durain have high DBF/F ratios (>0.68) and low DBT/F ratios (<1.28) (Fig. 10(b)). The distributions of DBT/F ratios in deltaic shale and coal were similar, but the DBF/F ratio of deltaic shale was lower (<0.65). Both carbonaceous shale and lagoonal shale exhibited high ratios of DBT/F ratios, and that of carbonaceous shale was higher (Fig. 10(b)). Overall, the cross plots of TeMNR vs. MNR and DBT/F ratios vs. DBF/F ratios serve as suitable indicators for distinguishing different lithologies for five types of coaly source rocks.

Large amounts of coaly-related petroleum reservoirs have been revealed around the world (Collinson et al., 1994; Wang et al., 2016; Zhao et al., 2018). Crude oil from younger Paleogene source rocks can be easily identified and quantified. However, the hydrocarbon potential of carbonaceous shale, lagoonal shale, and deltaic shale is underestimated, due to the lack of accurate methods for confirming the relationship between oil and coaly source rocks. This study indicates that the aromatic fraction of TeMNR, MNR, DBT/F ratios, and DBF/F ratios can well distinguish the characteristics of five types of coaly source rocks. These findings suggest that the estimation of crude oil and condensate can be determined by analyzing the source and evolution of different coaly source rocks. Our findings provide deeper insight into the hydrocarbon potential and coal–source for the associated rocks. This approach could be useful for exploring similar coaly source rocks in similar regions worldwide.

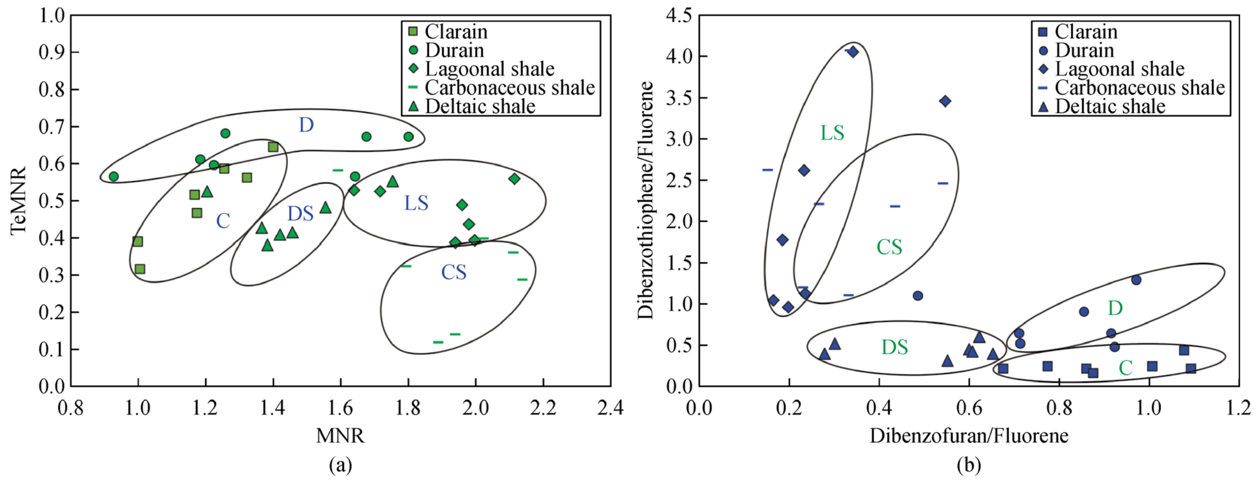

Fig. 10 Plots of TeMNR vs. MNR and Dibenzofuran/Fluorene vs. Dibenzothiophene/Fluorene for distinguishing lithologies (from thermal simulation). (a) parameters of naphthalene series compounds for discriminating different lithologies of coaly source rocks; (b) parameters of fluorene series compounds for discriminating different lithologies of coaly source rocks. TeMNR = 1,3,6,7-TeMN/[1,3,6,7 + 1,2,5,6-TeMN], C = clarain, D = durain, CS = carbonaceous shale, LS = lagoonal shale, DS = deltaic shale.

6 Conclusions

C–P coaly source rocks have significant hydrocarbon potential in the descending order of clarain, durain, carbonaceous shale, deltaic shale, and lagoonal shale. The clarain, durain, and carbonaceous shale were characterized by higher yield and the earlier peak of liquid hydrocarbon and more gas hydrocarbon than lagoonal and deltaic shales. Our results indicated that coaly source rock could provide significant hydrocarbon resources for the Bohai Bay Basin.

Although coaly source rocks accumulated abundant terrigenous organic matter, the high hydrocarbon potential of clarain, durain, and carbonaceous shale was attributed to sporinite and cutinite of liptinite and hydrogen-rich collodetrinite. In contrast, the lower hydrocarbon potential of lagoonal and deltaic shales can be caused by low hydrogen-rich maceral components (e.g., less exinite and hydrogen-poor vitrinite).

The coaly shales trended to produce the different composition of saturated hydrocarbons during the thermal evolution process, which was characterized by the Ts/(Ts + Tm), Ga/17α(H)21β(H)-C_{30} hopane, 18α(H)-oleanane/17α(H)21β(H)-C_{30} hopane, and 17β(H)21α(H)-C_{30} morane/17α(H)21β(H)-C_{30} hopane. Aromatic fraction, particularly parameters of fluorene and naphthalene, provided more beneficial information for differentiating coaly source rocks. Five lithologies of coaly source rocks can be identified from the TeMNR, MNR, DBT/F, and DBF/F. The discrimination supported by the fluorene and naphthalene compounds could be beneficial for revealing organic geochemical differences among coaly source rocks and coaly-related oils.

The prospect of coaly source rock potential provides a new direction of energy exploration for the most oil fields in the Bohai Bay Basin. A new perspective of using parameters of fluorene and naphthalene series compounds to identify the different lithotypes of coaly source takes new insight for source analysis between coaly-related oils and coaly source rocks deposited the similar environments worldwide.

Acknowledgements The work presented in this paper was supported by the Certificate of National Science and Technology Major Project of the Ministry of Science and Technology of China (No. 2016ZX05006-007-004), National Natural Science Foundation of China (Grant Nos. 41702139, 420772164, 42072130, and U1762217), Natural Science Foundation of Shandong Province (No. ZR2017BD036), the Fundamental Research Funds for the Central Universities (No. 18CX02008A), and Taishan Scholar Program of Shandong Province (No. TSQN201812030). We also thanks for the data support from PetroChina Dagang Oilfield Company.

References

Ahmed M, Volk H, George S C, Faiz M, Stalker L (2009). Generation and expulsion of oils from Permian coals of the Sydney Basin. Australia. Org Geochem, 40(7): 810–831

Asif M (2010). Geochemical applications of polycyclic aromatic hydrocarbons in crude oils and sediments from pakistan. Dissertation for Doctor Degree. Lahore: University of Engineering and Technology

Asif M, Alexander R, Fazeelat T, Pierce K (2009). Geosynthesis of dibenzothiophene and alkyl dibenzothiophenes in crude oils and sediments by carbon catalysis. Org Geochem, 40(8): 895–901

Chang J, Qiu N, Zhao X, Shen F, Liu N, Xu W (2018). Mesozoic and Cenozoic tectono-thermal reconstruction of the western Bohai Bay Basin (East China) with implications for hydrocarbon generation and migration. J Asian Earth Sci, 160: 380–395

Collinson M E, Van Bergen P F, Scott A C, De Leeuw J W (1994). The oil-generating potential of plants from coal and coal-bearing strata through time: a review with new evidence from Carboniferous plants. Geol Soc Lond Spec Publ, 77(1): 31–70

Colmenero J R, Suárez-Ruiz I, Fernández-Suárez J, Barba P, Llorens T (2008). Genesis and rank distribution of Upper Carboniferous coal basins in the Cantabrian Mountains, Northern Spain. Int J Coal Geol, 76(3): 187–204

D'Angelo J A, Zodrow E L, Camargo A (2010). Chemometric study of functional groups in Pennsylvanian gymnosperm plant organs (Sydney Coalfield, Canada): implications for chemotaxonomy and assessment of kerogen formation. Org Geochem, 41(12): 1312–1325

Figueiredo J J P, Hodgson D M, Flint S S, Kavanagh J P (2010). Depositional environments and sequence stratigraphy of an exhumed permian mudstone-dominated submarine slope succession, Karoo Basin, South Africa. Am J Bot, 60: 736–744

Greb S F, Martino R L (2005). Fluvial–Estuarine Transitions in Fluvial dominated Successions: Examples from the Lower Pennsylvanian of the Central Appalachian Basin. In: Blum M D, Marriott S B, Leclair S F, eds. Fluvial Sedimentology VII. IAS Special Publication 35: 425–451

Hartgers W A, Sinninghe Damste J S, de Leeuw J W, Ling Y, Dyrkacz G R (1994). Molecular characterization of flash pyrolyzates of two carboniferous coals and their constituting maceral fractions. Energy Fuels, 8(5): 1055–1067

He J, Ding W, Zhang J, Li A, Zhao W, Dai P (2016). Logging identification and characteristic analysis of marine–continental transitional organic-rich shale in the Carboniferous–Permian strata, Bohai Bay Basin. Mar Pet Geol, 70: 273–293

Hughes W B, Holba A G, Dzou L (1995). The ratios of dibenzothiophene to phenanthrene and pristane to phytane as indicators of depositional environment and lithology of petroleum source rocks. Geochim Cosmochim Acta, 59(17): 3581–3598

ICCP (International Committee for Coal and Organic Petrology) (1998). The new vitrinite classification (ICCP System 1994). Fuel, 77(5): 349–358

ICCP (International Committee for Coal and Organic Petrology) (2001). The new inertinite classification (ICCP System 1994). Fuel, 80(4): 459–471

ISO 7404–2 (2009). Methods for the Petrographic Analysis of Bituminous Coal and Anthracite-Part 2: Methods for Preparing Coal Samples. International Organization for Standardization, Geneva, Switzerland, 8

ISO 7404–3 (2009). Methods for the Petrographic Analysis of Coals-Part 3: Method of Determining Maceral Group Composition. International Organization for Standardization, Geneva, Switzerland, 18

ISO 7404–5 (2009). Methods for the Petrographic Analysis of Coals-Part 5: Method of Determining Microscopically the Reflectance of Vitrinite, Geneva, Switzerland, 14

Jin Q, Song G, Wang L (2009). Generation models of Carboniferous-Permian coal-derived gas in Shengli Oilfield. Pet Explor Dev, 36(3): 358–364

Kędzior S (2009). Accumulation of coal-bed methane in the south-west part of the Upper Silesian Coal Basin (southern Poland). Int J Coal Geol, 80(1): 20–34

Kim J (2001). Comparison of the Ordovician–Carboniferous boundary between Korea and NE China: implications for correlation and tectonic evolution. Gondwana Res, 4(1): 39–53

Li J G, Li M, Wang Z Y (2004). Dibenzofuran series in terrestrial source rocks and crude oils and applications to oil-source rock correlations in the Kuche Depression of Tarim Basin, NW China. Chin J Geochem, 23(2): 113–123

Li L, Li Z, Liu H J, Fang X Y (2015). Late Mesozoic to Cenozoic extension and strike slip structures and deep background of Bohai Bay Basin. Chinese Journal of Geology, 50: 446–472

Li M, Wang T, Zhong N, Zhang W, Sadik A, Li H (2013). Ternary diagram of fluorenes, dibenzothiophenes and dibenzofurans: Indicating depositional environment of crude oil source rocks. Energy Exploration & Exploitation, 31(4): 569–588

Li Y, Tang D, Wu P, Niu X, Wang K, Qiao P, Wang Z (2016). Continuous unconventional natural gas accumulations of Carboniferous-Permian coal-bearing strata in the Linxing area, northeastern Ordos basin, China. J Nat Gas Sci Eng, 36: 314–327

Li Y, Wang Z, Gan Q, Niu X, Xu W (2019a). Paleoenvironmental conditions and organic matter accumulation in Upper Paleozoic organic-rich rocks in the east margin of the Ordos Basin, China. Fuel, 252: 172–187

Li Y, Wang Z, Wu P, Gao X, Yu Z, Yu Y, Yang J (2019b). Organic geochemistry of Upper Paleozoic source rocks in the eastern margin of the Ordos Basin, China: input and hydrocarbon generation potential. J Petrol Sci Eng, 181: 106202

Li Y, Yang J, Pan Z, Tong W (2020). Nanoscale pore structure and mechanical property analysis of coal: an insight combining AFM and SEM images. Fuel, 260: 116352

Li Z X, Sun Y Z, Yu J F, Liu D Y (2001). Marine transgression "event" in coal formation from North China Basin. Energ Energ Explor & Exploit, 19(6): 559–567

Liu G (1990). Permo-Carboniferous paleogeography and coal accumulation and their tectonic control in the north and south China continental plates. Int J Coal Geol, 16(1–3): 73–117

Luo J, Cheng K, Fu L (2001). Alkylated dibenzothiophene index: a new method to assess thermal maturity of source rocks. Acta Petrol Sin, 22(3): 27–32

Lv D, Chen J (2014). Depositional environments and sequence stratigraphy of the Late Carboniferous-Early Permian coal-bearing successions (Shandong Province, China): sequence development in an epicontinental basin. J Asian Earth Sci, 79: 16–30

Mello M R, Gaglianone P C, Brassell S C, Maxwell J R (1988). Geochemical and biological marker assessment of depositional environments using Brazilian offshore oils. Mar Pet Geol, 5(3): 205–223

Michelsen J K, Khorasani G K (1990). Monitoring chemical alterations of individual oil-prone macerals by means of microscopical fluorescence spectrometry combined with multivariate data analysis. Org Geochem, 15(2): 179–192

Peters K E, Cassa M R (1994). Applied source rock geochemistry. In: Magoon L B, Dow W G, eds. The Petroleum System–From Source to Trap: AAPG Memoir 60: 93–117

Petersen H I, Andsbjerg J, Bojesen Koefoed J A, Nytoft H P (2000). Coal‐generated oil: source rock evaluation and petroleum geochemistry of the Lulita oilfield, Danish North Sea. J Pet Geol, 23(1): 55–90

Pickel W, Kus J, Flores D, Kalaitzidis S, Christanis K, Cardott B J, Misz-Kennan M, Rodrigues S, Hentschel A, Hamor-Vido M, Crosdale P, Wagner N (2017). Classification of liptinite- ICCP system 1994. Int J Coal Geol, 169: 40–61

Radke M, Vriend S P, Ramanampisoa L R (2000). Alkyldibenzofurans in terrestrial rocks: influence of organic facies and maturation. Geochim Cosmochim Acta, 64(2): 275–286

Radke M, Willsch H (1994). Extractable alkyldibenzothiophenes in Posidonia Shale (Toarcian) source rocks: relationship of yields to petroleum formation and expulsion. Geochim Cosmochim Acta, 58 (23): 5223–5244

Ryder R T, Jin Q, McCabe P J, Nuccio V F, Persits F (2012). Shahejie–Shahejie/Guantao/Wumishan and Carboniferous/Permian coal–Paleozoic total petroleum systems in the Bohaiwan Basin, China (based on geologic studies for the 2000 World Energy Assessment Project of the US Geological Survey). US Geological Survey, Reston, Virginia

Stasiuk L D (1994). Oil-prone alginite macerals from organic-rich Mesozoic and Palaeozoic strata, Saskatchewan, Canada. Mar Pet Geol, 11(2): 208–217

Suwarna N (2006). Permian Mengkarang coal facies and environment, based on organic petrology study. Indonesian J Geosci, 1: 1–8

Tang X, Zhang J, Shan Y, Xiong J (2012). Upper Paleozoic coal measures and unconventional natural gas systems of the Ordos Basin, China. Geosci Front, 3(6): 863–873

Tewari R C, Khan Z A (2015). Origin of banded structure and coal lithotype cycles in Kargali coal seam of East Bokaro sub-basin, Jharkhand, India: environmental implications. J Earth Syst Sci, 124(3): 643–654

Wang D D, Shao L Y, Li Z X, Li M P, Lv D, Liu H (2016). Hydrocarbon generation characteristics, reserving performance and preservation conditions of continental coal measure shale gas: a case study of Mid-Jurassic shale gas in the Yan'an Formation, Ordos Basin. J Petrol Sci Eng, 145: 609–628

Wei Z B, Zhang D J, Zhang C L, Chen J P (2001). Methyldibenzothiophenes distribution index as a tool for maturity assessments of source rocks. Geochim Cosmochim Acta, 30(3): 242–248

Xu J J, Jin Q (2020). Hydrocarbon potential and polycyclic aromatic compounds differences of Carboniferous–Permian coaly source rocks, Bohai Bay Basin: an implication for different sources of gas condensate and oils. J Petrol Sci Eng, 195: 107899

Zeng L B, Su H, Tang X M, Peng Y M, Gong L (2013). Fractured tight sandstone oil and gas reservoirs: a new play type in the Dongpu depression, Bohai Bay Basin, China. AAPG Bull, 97(3): 363–377

Zhao X, Jin F, Wang Q, Bai G (2015). Buried-hill play, Jizhong subbasin, Bohai Bay basin: a review and future prospectivity. AAPG Bull, 99: 1–26

Zhao X, Zhou L, Pu X, Jiang W, Jin F, Xiao D, Han W, Zhang W, Shi Z, Li Y (2018). Hydrocarbon-generating potential of the Upper Paleozoic section of the Huanghua Depression, Bohai Bay Basin, China. Energy Fuels, 32(12): 12351–12364

Zhou L, Fu L, Lou D, Lu Y, Feng J, Zhou S, Santosh M, Li S (2012). Structural anatomy and dynamics of evolution of the Qikou Sag, Bohai Bay Basin: implications for the destruction of North China craton. J Asian Earth Sci, 47: 94–106